MEASUREMENTS AND SIMULATIONS IN HIGH ENERGY NEUTRON FIELDS

C. Birattari [#], E. De Ponti [#], A. Esposito*, A. Ferrari [†],
M. Magugliani [#], M. Pelliccioni*, T. Rancati [#], M. Silari°

Abstract

The application of the FLUKA Monte Carlo code in the simulation of particle cascades in the shielding of the H6 beam in the SPS North Experimental Hall (CERN) has been tested against experimental results. The present paper demonstrates the validity of the code in predicting neutron spectra in very complex geometrical conditions with large attenuation factors involved. The same experimental data served as a confirmation of the behaviour of a modified Andersson-Braun rem counter with a response function extended up to hundreds of MeV (LINUS).

[#] **Universit a di Milano, Dipartimento di Fisica**, LASA,
Via Fratelli Cervi 201, 20090 Segrate, Italy.

* **Istituto Nazionale di Fisica Nucleare, Laboratori Nazionali di Frascati**,
00044 Frascati, Italy.

[†] **Istituto Nazionale di Fisica Nucleare, Sezione di Milano**,
Via Celoria 16,
20133 Milano, Italy.

° **Consiglio Nazionale delle Ricerche, Istituto Tecnologie Biomediche Avanzate**
Via Ampere 56, 20131 Milano, Italy.

1. Introduction

Three series of measurements in high energy stray radiation fields were performed at CERN in July 1993, May 1994 and April 1995. These measurements were carried out at the beam line H6 from the Super Proton Synchrotron (SPS), in the North Area of the Prevessin site, where a reference facility for high energy neutron dosimetry studies is available. Several European (and also from outside Europe) laboratories participated with dosimeters and spectrometers in these field investigations, organised within the framework of a CERN-CEC collaboration.

The INFN Milan and Frascati groups participated with the rem counters SNOOPY (a standard Andersson-Braun rem counter) and LINUS (a new rem counter) and with 5 polyethylene cylinders of different size having at their centre a BF_3 proportional counter. The bare BF_3 counter and the counter under a cadmium cover were also used.

These measurements were performed to test the response of the two rem counters in high energy neutron fields and to allow a comparison between field measurements and Monte Carlo simulations performed using the FLUKA code. The polyethylene cylinders were also used to get an experimental estimate of the neutron spectrum (each cylinder being capable of detecting neutrons belonging to different energy regions).

A description of the experimental conditions is given in section 2, while the Monte Carlo simulations are discussed in section 3. In particular, section 3.1 refers to the simulation of the response function of the detecting devices while section 3.2 deals with the simulation of the CERN test beam set up. The experimental data and the Monte Carlo results are compared and discussed in section 4.

2. Experimental setup

The beam consisted of 205 GeV/c positively charged particles (about 2/3 protons and 1/3 pions). This beam was shot at the centre of a cylindrical copper target (50-cm length, 7-cm diameter) which was located either under a 40-cm thick iron roof shield ("iron" position) or under a 80-cm thick concrete roof shield ("concrete" position). The arrangement of the shielding blocks around the target area is shown in Figures 1 and 2 where the measurement positions are also indicated. All the shields were made by concrete blocks ($240\times160\times80$ cm^3) except the roof above the iron position.

During the three experimental runs measurements were performed at a number of locations around the shieldings. These locations are divided into four groups according to the following classification:

- CONCRETE TOP,
- CONCRETE SIDE,
- IRON TOP and
- IRON SIDE (the last group refers to the condition with the target placed under the iron roof but measurements made behind a 160-cm concrete side wall).

Measurement positions are listed in Table 1. The beam monitoring was provided by CERN by means of a Precision Ionization Chamber (PIC) [1]. One count of this instrument was estimated with independent methods to correspond to 2.2×10^4 ±10% (the error is systematic) primary particles incident on the target. All the data presented in this paper are normalised to one PIC count.

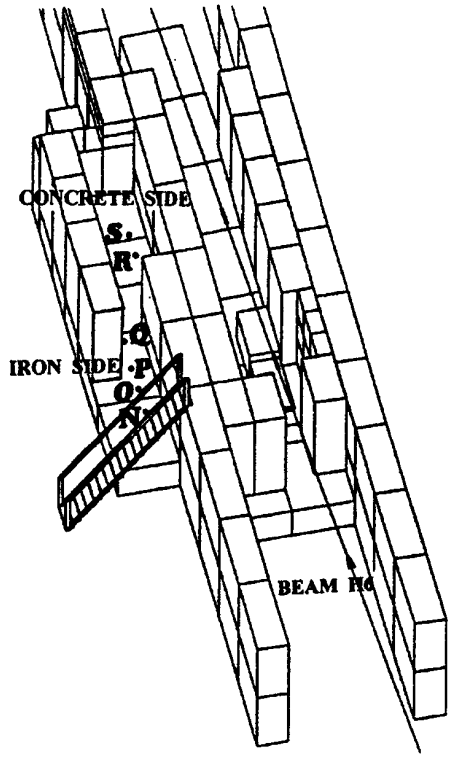

Figure 1 ***Axonometric view of the target area and lateral shielding. The top shieldings are removed.***

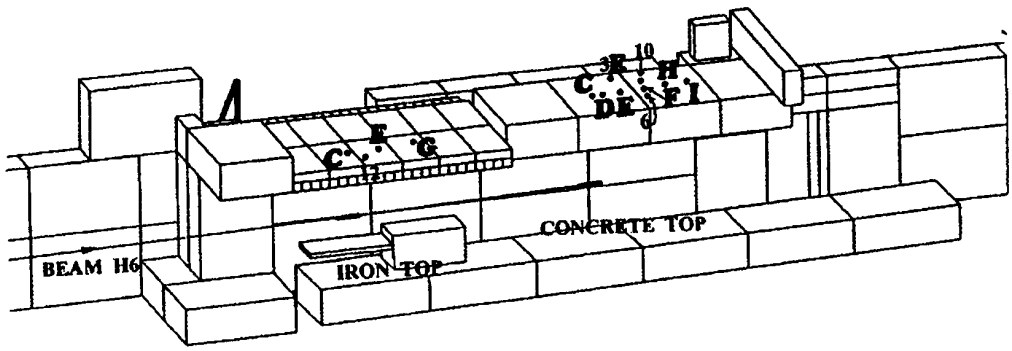

Figure 2 ***Axonometric side view of the target area, with the lateral shielding removed.***

Table 1 ***Measurements positions***

POSITION GROUP	SHORT NAME	DISTANCE TO SHIELDING	DOWNSTREAM DISTANCE FROM TARGET	POSITION WITH RESPECT TO THE BEAM DIRECTION
CONCRETE TOP	C	25 cm	0 cm	aligned
	D	25 cm	25 cm	aligned
	E	25 cm	75 cm	aligned
	3E	25 cm	75 cm	100 cm left
	F	25 cm	125 cm	aligned
	6	25 cm	125 cm	125 cm right
	10	25 cm	125 cm	125 cm left
	H	25 cm	175 cm	aligned
	I	25 cm	213 cm	aligned
IRON TOP	C	25 cm	0 cm	aligned
	E	25 cm	75 cm	aligned
	G	25 cm	150 cm	aligned
	12	25 cm	25 cm	25 cm right
POSITION GROUP	**SHORT NAME**	**DISTANCE TO SHIELDING**	**DOWNSTREAM DISTANCE FROM TARGET**	**HEIGHT WITH RESPECT TO BEAM**
CONCRETE SIDE	R	50 cm	-125 cm	0 cm
	S	50 cm	0 cm	0 cm
IRON SIDE	N	50 cm	0 cm	0 cm
	O	50 cm	100 cm	0 cm
	P	50 cm	200 cm	0 cm
	Q	50 cm	340 cm	0 cm

3. Monte Carlo simulations

Monte Carlo simulations were carried out with the last version of the FLUKA code (see [2,3,4,5,6,7] and references therein). The present version of the code has been developed in Milan and includes the capability of transporting also low energy neutrons ($E_n < 20$ MeV) using a multigroup cross-section library especially developed for FLUKA [8].

Calculations were performed using a three-step procedure:

- First, the detector response functions were calculated;
- Second, the neutron fluences at the measurement positions were computed; and,
- Third, the computed responses to monoenergetic neutron beams were folded with the scored fluences.

3.1 Calculation of the response functions

In order to compute the fluence response of the various devices each monitor was represented using the combinatorial geometry and the detector and the surrounding attenuator/moderator were reproduced

as accurately as possible. A track length estimator corresponding to the effective volume of the BF_3 counter was used for scoring. Its response function was the same as that of the B-10 (n,α) reaction.

Three kinds of response functions were considered: lateral and isotropic irradiation for energies below 20 MeV and lateral irradiation for energies above 20 MeV. By lateral irradiation we mean irradiation by a uniform and parallel radiation field (a situation which corresponds to the conditions under which the ambient dose equivalent is calculated). In isotropic irradiation an isotropic neutron fluence around the detectors was simulated. These two kinds of irradiations were chosen in order to allow the use either of a single response function or of an appropriate mix of both, according to the angular distribution of the neutrons striking the detector.

For LINUS and SNOOPY only the lateral response function was calculated because of their low sensitivity to low energy neutrons. In all the experimental conditions presented in this paper high and intermediate energy neutrons can be considered as striking the detectors laterally, while angular distributions become nearly isotropic for decreasing neutron energies (see also section 3.2): these low energy neutrons arise from a great number of interactions and do not record the direction of the primary particle from which they derive. For the same reason no isotropic response above 20 MeV was calculated. Looking carefully at the computed response functions one can see that the anisotropy of the response becomes smaller with increasing energy and vanishes above 10 MeV.

Below 20 MeV use was made of the multigroup cross-section data sets, with 72-neutron energy groups in the energy range from thermal to 20 MeV [8]. In this range the histogram representation of the response function curves presented in the following reflects the group structure of the cross-section data sets. Above 20 MeV lateral irradiation with monoenergetic neutrons was simulated. Sixteen energies (from 21 MeV up to 2 GeV) were considered. In the following the detectors are described and their computed response functions are presented. These response functions are also given numerically in the Annex, Tables 13-17.

All simulations were carried out on a DEC Alpha 3000/600 workstation running Open VMS 6.1. The average CPU time per primary particle depends on the device and the neutron energy considered:

- For LINUS (which is the most complex device) it is about 2×10^{-2} s (E<20 MeV), 2.5×10^{-2} s (E<25 MeV), and 8×10^{-2} s (E<2 GeV), and,
- For cylinder 2 it is about 3×10^{-3} s (E<20 MeV), 8×10^{-4} s (E<25 MeV), and 10^{-3} s (E<2 GeV).

The number of primary particles required to achieve statistical errors of few percent was about 10^7 for energies below 20 MeV (the 72 groups were handled at the same time) and about 10^4 – 10^5 (single energy) above 20 MeV.

3.1.1 The rem counters LINUS and SNOOPY

A rem counter consists of a detector with a high efficiency for thermal neutrons placed inside a moderator/attenuator structure such that the response function of the instrument reproduces as faithfully as possible the curve of the conversion coefficients from neutron fluence to ambient dose equivalent -H*(10) – over a wide energy range.

SNOOPY is a conventional Andersson-Braun rem counter [9]. It consists of a BF_3 proportional counter of 2.54-cm diameter and 5.08-cm nominal active length (95% B-10 enrichment, fill pressure 8.0×10^4 Pascal) surrounded by: an inner polyethylene moderator (1.9 cm thick), a boron doped synthetic rubber attenuator (7.6 cm outer diameter, 14 cm length and 0.6 cm thickness) and an outer polyethylene moderator (21.7 cm outer diameter, 23.9 cm length and 7 cm thickness). A number of holes are drilled in both the lateral and front surfaces of the boron plastic attenuator in order to allow some of the thermal neutrons to penetrate. The area of the holes covers about 20% of the boron attenuator total area. Figure 3 shows a longitudinal cross-section of the instrument as it was coded into the computer.

The SNOOPY response is considered acceptable for radiation protection purposes for neutron energies from thermal to 14 MeV. For energies above 14 MeV its response becomes inadequate: its sensitivity drops and the instrument underestimates the ambient dose equivalent [10].

LINUS (Long Interval NeUtron Survey-meter) is an extended range version of SNOOPY. A lead layer (1 cm thick) has been placed between the boron-doped synthetic rubber attenuator and the outer polyethylene moderator. Lead has no significant effect at energies below 10 MeV, while the fluence response is highly increased above 10 MeV (at 14 MeV its response is about 40% larger than that of SNOOPY and about 55% larger at 19 MeV) (for details see [10,11,12]). Figure 4 shows a longitudinal cross-section of the new rem counter as described in combinatorial geometry.

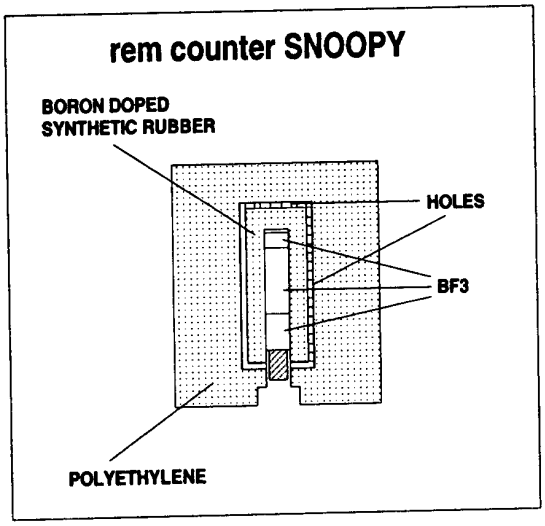

Figure 3 ***Rem counter SNOOPY. Longitudinal cross-section.***

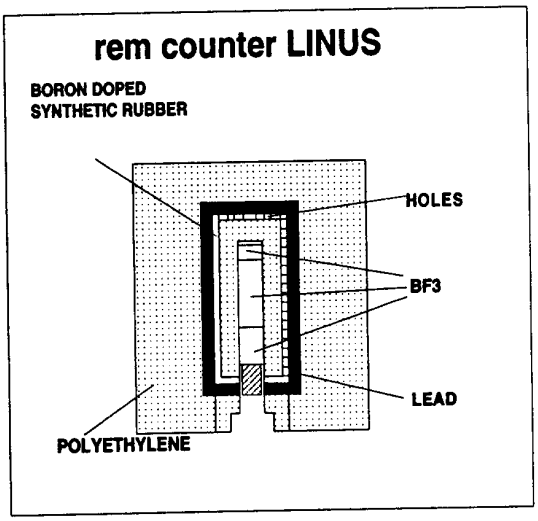

Figure 4 ***Rem counter LINUS. Longitudinal cross-section.***

The improved rem counter LINUS has already been tested in high energy stray radiation fields in two previous experiments at CERN 13,14] and has been calibrated with monoenergetic neutrons in the range from thermal to 19 MeV provided by the Physikalische-Technische Bundesanstalt (PTB) in Braunschweig (Germany) [12,14]. Measurements with nearly monoenergetic neutron fields at 39.5,

50, 60.7 and 70 MeV were also performed at the Paul Scherrer Institute (PSI) in Villigen (Switzerland) [14] (the energies are those of the protons hitting the beryllium target).

The computed response for the LINUS counter together with the H*(10) curve and the experimental values resulting from the PTB calibration are drawn in Figure 5. The dashed lines correspond to one (calculated) standard deviation statistical error. The energy scale on the horizontal axis has been split in correspondence to 10^5 eV in order to expand and better show the high energy region. When plotting the H*(10) curve we have chosen the conversion coefficients from neutron fluence to ambient dose equivalent proposed in [15,16]. The computed response for the SNOOPY counter is drawn in Figure 6. The curves in Figures 5 and 6 have been drawn according to a nominal sensitivity referred to a sensitive volume and a pressure of the filling gas of the BF^3 counter as given above.

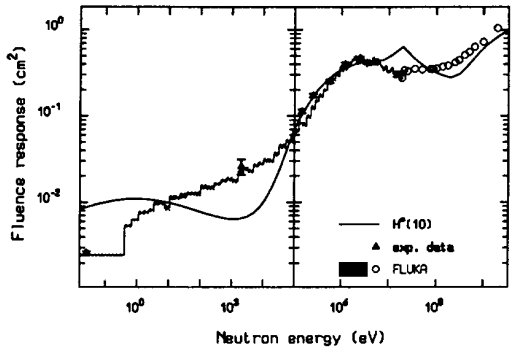

Figure 5 ***Rem counter LINUS. Fluence response***

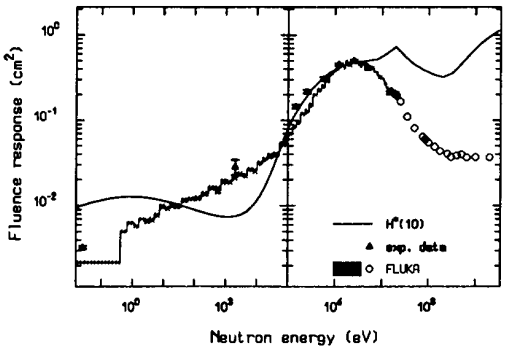

Figure 6 ***Rem counter SNOOPY. Fluence response***

As one can see the LINUS response function shows a marked increase at high energies (when compared with the SNOOPY response function) and no significant change in the other regions. There is also good agreement between the calculated response function and the experimental calibration points.

3.1.2 Polyethylene cylinders

The five high-density (0.96 g/cm^3) polyethylene cylinders are shown in Figure 7. Their diameters range from 7.8 cm to 22.8 cm. The thickness of the lateral polyethylene is: 2.55 cm (cylinder 1), 3.85 cm (cylinder 1B), 5.05 cm (cylinder 2), 7.55 cm (cylinder 3) and 10.5 cm (cylinder 4). The top and bottom thicknesses are the same but for cylinder 1B (5 cm).

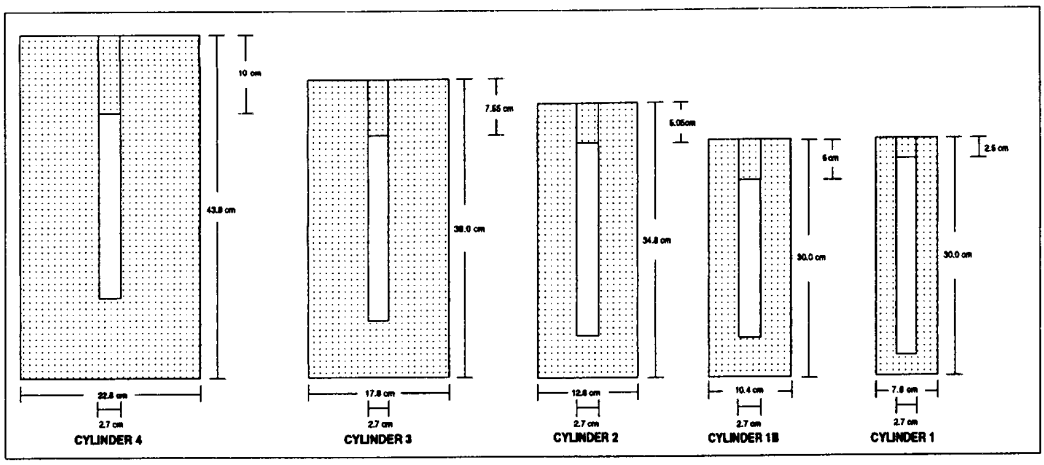

Figure 7 ***Polyethylene cylinders. Longitudinal cross-section***

Figures 8-12 show the response functions of the five cylinders. These detectors are especially sensitive to energies ranging from 10 eV (cylinder 1) up to 2 MeV (cylinder 4).

3.1.3 Bare BF_3 proportional counter

For the bare counter no fluence response was calculated: the curve of the B-10 (n,α) cross-section versus energy was adopted. This curve is shown in Figure 13. The maximum sensitivity is obviously reached at thermal energy.

3.1.4 BF_3 proportional counter under a cadmium cover

Also for the BF_3 proportional counter covered with a cadmium layer no fluence response was computed. The same response function of the bare counter was adopted for energies above 0.414 eV. For energies below 0.414 eV a zero response was assumed. In this energy range the cadmium cross-section is indeed very large.

3.2 Simulation of the CERN experimental set up

The CERN-CEC experimental area was modelled using the combinatorial geometry. Because of lack of information, the concrete composition was assumed to be a standard one, as reported in nuclear reactor guidelines. In particular Portland concrete was chosen with composition (weight fractions): 52.9% oxygen, 33.7% silicon, 4.4% calcium, 3.4% aluminium, 1.6% sodium, 1.4% iron, 1.3% potassium, 1% hydrogen, 0.2% magnesium and 0.1% carbon. The iron roof consisted of two layers with different average densities: upper-layer 7.2 g/cm^3, lower-layer 7.65 g/cm^3. These densities were determined by weighting a few blocks.

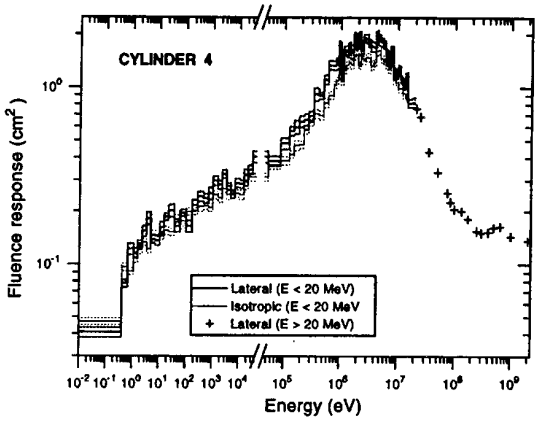

Figure 8: Cylinder 4. Fluence response.

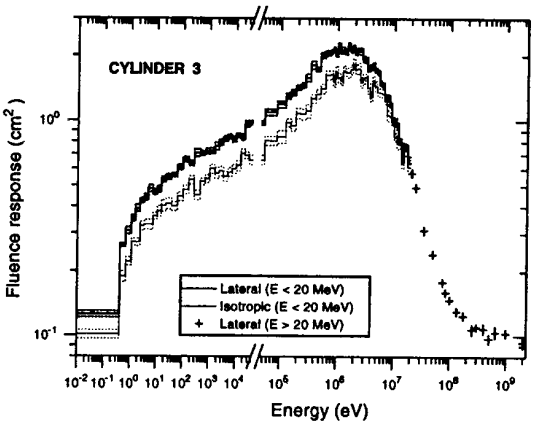

Figure 9: Cylinder 3. Fluence response.

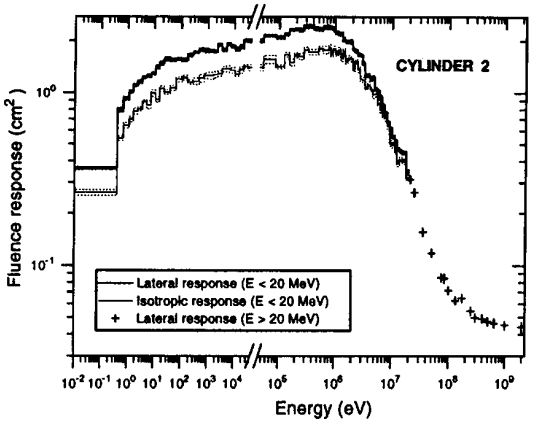

Figure 10: Cylinder 2. Fluence response.

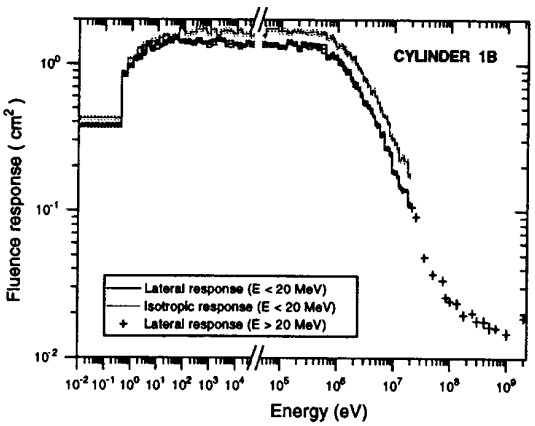

Figure 11: Cylinder 1B. Fluence response.

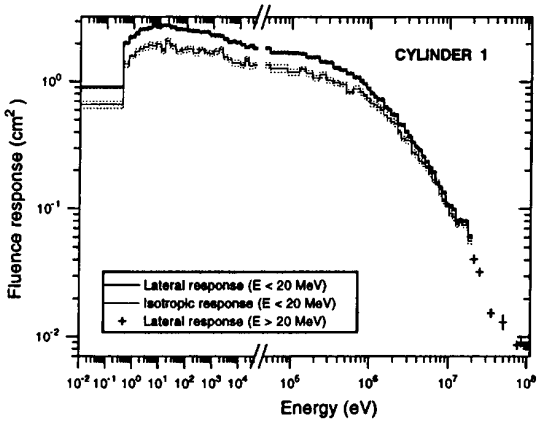

Figure 12: Cylinder 1. Fluence response.

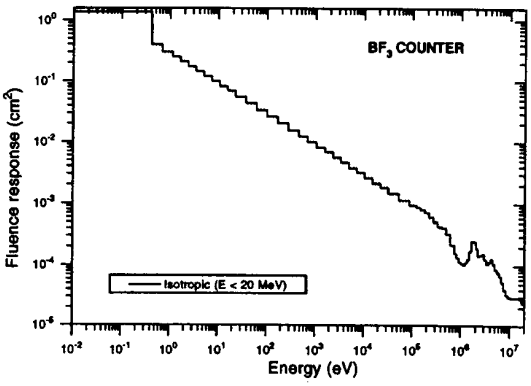

Figure 13: Bare counter. Fluence response.

According to the experimental conditions a beam consisting of 2/3 protons and 1/3 positive pions with a FWHM of 2.8 and 2.1 cm in the horizontal and vertical plane respectively was used in the simulations. All particle but electrons, positrons and photons were tracked through the geometry until they were absorbed or escaped from the system. Electromagnetic particles were discarded because of no interest for the present problem.

Two scoring spheres (24 cm and 40 cm diameter) were inserted in the geometry in each experimental measurement point. When this was not possible (because of overlapping with other regions) either the diameters were suitably reduced or only one sphere was considered. When two scoring regions were available the neutron fluence in the largest one was chosen because of better statistics. If a strong gradient was present the neutron fluence in the internal region was considered. The neutron fluences scored in some measurement positions are shown in Figures 14 and 15.

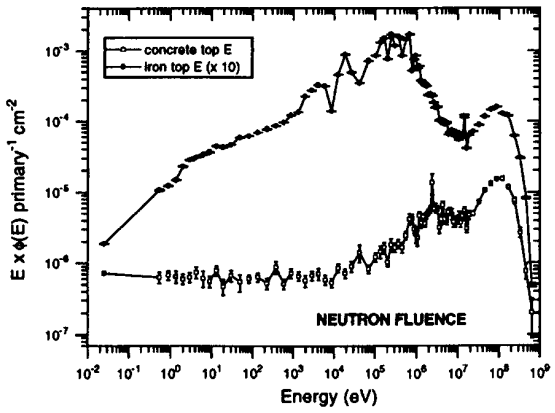

Figure 14 ***Concrete top (E) and iron top (E) positions. Neutron fluence as resulting from calculations.***

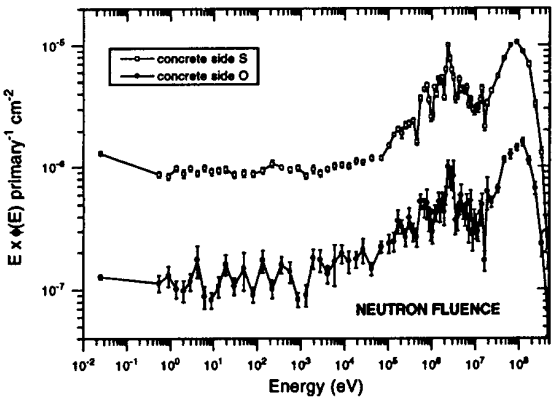

Figure 15 ***Concrete side (S) and iron side (O) positions. Neutron fluence as resulting from calculations.***

In order to better understand and reproduce the neutron fluence present at experimental locations the angular distribution of neutrons as a function of energy was also calculated. This information allowed us to determine (for each energy group and for each experimental position) a suitable figure r, to represent the degree of anisotropy of the neutron beam. This number is the fraction of neutron fluence which has to be folded with the detector isotropic response function, while the fraction $(1-r)$ is folded with the lateral response function. As already expected, r increases with decreasing neutron energies and it is ≈ 1 for the thermal group. For this reason for the two rem counters LINUS and SNOOPY only the lateral response function was considered (their sensitivity to thermal neutron is very low) and, on the other hand, for the bare proportional counter only the isotropic response function was used (it practically detects only thermal neutrons).

The number r has been determined as explained in the following. The Monte Carlo code has been used to calculate a double differential distribution of neutron fluence in energy and solid angle (angular distributions are intended as distributions in $\cos.\theta$, where θ is the angle between the particle trajectory and the normal to the shielding at the point of crossing). For each energy group 60 angular

trajectory and the normal to the shielding at the point of crossing). For each energy group 60 angular groups were considered. We chose to considered all neutrons crossing the shielding with 48°< θ<180° (angular groups from 11 to 60) as belonging to the isotropic fluence (I). The neutrons belonging to the first ten angular groups were considered as contributing to the lateral fluence (L). The figure r has been calculated from the expression $r = \frac{I}{I+L}$. The choice of the groups contributing to isotropic and lateral response is somewhat arbitrary and the whole procedure could be improved.

In order to save computing time extensive use of variance reduction techniques was made. Importance biasing at boundaries and energy dependent weight windows were applied in order to favour particle streaming towards the detector locations and not to waste CPU time following particles with a little probability of giving a contribution. The typical CPU time was about 18 s per primary particle. About 10^4 particles were tracked in order to obtain adequate statistics.

3.3 Folding and simulation results

The previously computed response of the counting devices to monoenergetic neutrons were finally folded with the fluxes scored at the measurement positions and the estimated number of counts per PIC was obtained. The results are given in the next section (Tables 3-10) together with the experimental counts.

For the polyethylene cylinders three simulated results are given. They correspond to three different kinds of folding: lateral response only, isotropic response only and the mix deriving from considering the angular distribution of neutrons through the r number discussed above (Section 3.1).

4. Experimental results and discussion

4.1 Calibration factor

All results presented in this paper (both experimental and calculated) are given for a BF_3 proportional counter whose sensitive volume and gas fill pressure are the nominal ones (see Section 3.1.1). The actual efficiencies of the BF_3 counters used in the experimental measurements are usually different from the nominal one and they were found to be not stable with time. One of the BF_3 counters was therefore calibrated at PTB in 1991 (exposing it to monoenergetic neutrons and to a calibrated Am-Be source) inside the LINUS and SNOOPY rem counters [12,14]. From this calibration the actual efficiency of this BF_3 counter at the time of the calibration was known and the following time evolution was monitored exposing it to an Am-Be source in standard conditions at the Laboratorio Acceleratori Superconduttivit a Applicata (LASA) in Milan (see Section 4.2). Of course the same calibration provided an intercalibration of the LASA source, which is now our standard reference when calibrating the counters.

Therefore from 1991 on, efficiency fluctuations are controlled through routine tests performed at LASA. This allows to determine (for each BF_3 counter) a factor K which takes the difference between "nominal" and real efficiency into account ("nominal" refers to the efficiency of a BF_3 counter with sensitive volume, gas pressure and B-10 enrichment corresponding to those given in Section 3.1) and which is used to normalise all the experimental results presented in this paper. For the PTB calibrated

tube this K factor was 0.74 ± 0.03 in 1991, 0.75 ± 0.05 in July 1993, 0.78 ± 0.05 in May 1994 and 0.76 ± 0.05 in April 1995. The other BF_3 counters have different K factors.

The ambient dose equivalent calibration factor S was established using the PTB calibration points. It comes from the ratio between the rem counter fluence response and the fluence to ambient dose equivalent conversion coefficients. For an ideal rem counter S would be the same in the whole energy range considered. For LINUS and SNOOPY it slightly varies; we chose an average value: 1.044 cts/nSv ± 8.0% for the rem counter LINUS and 1.209 cts/nSv ± 9.5% for SNOOPY (the quoted errors give an indication of the variation of S with energy). These values refer to a counter whose sensitivity is the nominal one.

4.2 Time stability of the counter

Since it was not possible to control the stability of the proportional counters during the CERN measurements, tests were performed at LASA before and after each measurement period. During these tests the detectors were exposed to an Am-Be source. The source emission rate is 2.3×10^6 n/s (±4%) (the source was intercalibrated with a PTB Am-Be source as explained above). The source was placed 3 m above the concrete floor, all other walls being at much larger distances. The detectors sat on a plexiglas support, with their centre at 2 m from the source. The neutron fluence rate at the measurement location was 4.58 n/cm^2/s ±4%. The LASA measurement geometry is shown in Figure 16. Simulations of this experimental set up were also carried out.

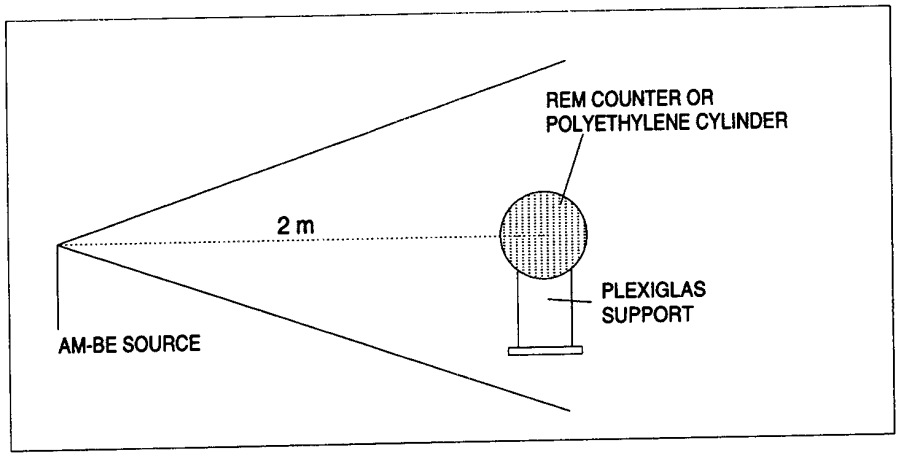

Figure 16 ***LASA geometry as described in the simulations***

Prior and following each experimental run the counters were exposed to the Am-Be source. This allowed to control that no significant change occurred and to establish a reference efficiency for the CERN period. For each counter the ratio between the LASA response and the response obtained with the calibrated tube in 1991 is assumed to be the ratio between the corresponding counting efficiencies. This ratio allows to refer to the PTB calibration efficiency and to normalise all results to a counter whose efficiency is the nominal one. Table 2 gives the LASA response (1995) together with the simulated response. The experimental results are reported to the nominal efficiency.

Table 2 ***LASA response. Experimental and computed results. Statistical errors only are shown***

DETECTOR	EXPERIMENTAL		FLUKA	
	cm^2	err%	cm^2	err%
LINUS	0.349	0.4	0.374	0.6
SNOOPY	0.354	0.3	0.398	0.5
CYLINDER 4	1.44	0.1	1.42	2.2
CYLINDER 3	1.54	0.1	1.51	1.9
CYLINDER 2	1.29	0.1	1.23	2.0
CYLINDER 1B	0.898	0.5	0.872	2.1
CYLINDER 1	0.387	0.2	0.414	2.5

4.3 Experimental results

The experimental and the computed results are presented in Tables 3-10. The quoted errors are only statistical and do not include systematic uncertainties in the beam monitoring (which are estimated to be 10%) and in the efficiency of the BF_3 counter (5%).

Experimental data were collected in different years. In general there is no great difference among them; in this case the 1995 results are reported. When important differences were found, the data obtained in other years are also presented. As one can see, the agreement between experimental and simulated counts is fairly good. It should be stressed that the problem is very complex and uncertainties are not negligible. The major differences between simulated and experimental counts were found for the bare counter (iron positions) and for the counter under the cadmium cover (1995 measurements). The bare counter is extremely sensitive to thermal neutrons. The presence of moderating materials modifies the thermal portion of the spectrum. As it is shown by the sequence of measurements presented in Table 9, the counts coming from the bare counter are quite dependent on the presence of other (polyethylene) detectors near it. When the measurement area was left free, the response of the counter dropped and it came closer to the computed one. This fact shows that the problem came from the experimental area overcrowding. For the concrete positions *a* significant uncertainty on the simulated counts for the bare counter is due to the unknown concrete composition. The actual intensity of the thermal neutron spectrum is strongly dependent on concrete composition and it has great importance for a device which practically detects only thermal neutrons.

On the other hand the counter under the cadmium cover is insensitive to thermal neutrons because of the high cadmium neutron cross-section at these energies. Here a problem rises when the cover is not tightly sealed: This allows some thermal neutrons to penetrate and be detected. Concrete positions are especially critical. Here a great number of thermal neutrons are present and a small aperture in the cadmium cover can cause a lot of them to be detected.

Table 3 ***LINUS and SNOOPY. CERN experimental and computed results. Statistical errors only are shown.***

POSITION	LINUS				SNOOPY			
	EXPERIMENTAL		FLUKA		EXPERIMENTAL		FLUKA	
	cts/PIC	err%	cts/PIC	err%	cts/PIC	err%	cts/PIC	err%
CONCRETE TOP								
C	0.268	0.62	0.281	2.4	0.156	0.78	0.153	2.4
E	0.364	0.36	0.391	2.8	0.200	0.59	0.201	3.1
F	0.362	0.35	0.367	3.1	0.209	0.52	0.201	3.8
I	0.319	0.56	0.367	2.2	0.174	0.78	0.184	2.1
6	0.359	0.54	0.400	2.3	0.199	0.72	0.200	2.2
10	0.379	0.54	0.401	1.9	0.214	0.69	0.202	1.9
CONCRETE SIDE								
R	0.154	0.29	0.141	2.3	0.113	0.16	0.094	2.2
S	0.316	0.45	0.299	2.1	0.214	0.56	0.182	1.9
IRON TOP								
C	1.78	0.30	1.52	1.9	1.83	0.75	1.49	1.9
E	2.12	0.11	1.87	2.0	2.16	0.27	1.79	2.1
G	1.65	0.65	1.60	2.2	1.69	0.68	1.50	2.1
IRON SIDE *								
N	0.0268	2.1	0.0259	3.6	-	-	-	-
O	0.0414	1.8	0.0398	3.0	0.0297	2.4	0.0216	3.8
P	0.0545	1.8	0.0543	3.1	-	-	-	-
Q	0.0865	1.2	0.0908	2.9	-	-	-	-
R	0.194	0.65	0.193	2.6	-	-	-	-
S	0.156	1.0	0.155	2.7	-	-	-	-

* 1993 measurements.

Table 4 ***CYLINDER 4. CERN experimental and computed results. Statistical errors only are shown***

POSITION	EXPERIMENTAL		FLUKA-ISOTROPIC		FLUKA-MIXTURE		FLUKA-LATERAL	
	cts/PIC	err%	cts/PIC	err%	cts/PIC	err%	cts/PIC	err%
CONCRETE TOP								
C	0.541	0.29	0.555	2.3	0.593	2.3	0.647	2.3
D	0.723	0.36	0.583	3.7	0.640	3.7	0.731	3.7
E	0.700	0.24	0.728	2.8	0.782	2.8	0.843	2.8
F	0.871	0.62	0.657	3.5	0.736	3.5	0.822	3.5
H	0.819	0.47	0.678	2.7	0.754	2.7	0.846	2.7
3E	0.568	0.50	0.459	3.1	0.509	3.1	0.541	3.1
CONCRETE SIDE								
R	0.331	0.31	0.352	2.1	0.380	2.21	0.414	2.1
S	0.709	0.49	0.674	1.9	0.721	1.9	0.790	1.9
IRON TOP								
C	6.84	0.15	6.04	1.9	6.83	1.9	7.53	1.9
E	7.53	0.15	7.08	2.1	8.03	2.1	8.83	2.1
12	7.41	0.29	5.37	2.1	7.55	2.1	6.51	2.1

Table 5 ***CYLINDER 3. CERN experimental and computed results. Statistical errors only are shown.***

POSITION	EXPERIMENTAL		FLUKA-ISOTROPIC		FLUKA-MIXTURE		FLUKA-LATERAL	
	cts/PIC	err%	cts/PIC	err%	cts/PIC	err%	cts/PIC	err%
CONCRETE TOP								
C	0.683	0.45	0.631	2.3	0.685	2.3	0.772	2.3
D	0.870	0.36	0.703	3.4	0.768	3.4	0.880	3.4
E	0.886	0.32	0.820	2.9	0.899	2.9	0.995	2.9
F	1.08	0.59	0.789	3.8	0.878	3.8	0.990	3.8
H	1.02	0.39	0.815	2.8	0.906	2.8	1.02	2.8
3E	0.691	0.43	0.549	3.1	0.609	3.1	0.687	3.1
CONCRETE SIDE								
R	0.484	0.38	0.453	2.1	0.497	2.1	0.570	2.1
S	0.972	0.07	0.831	1.9	0.908	1.9	1.04	1.9
IRON TOP								
C	13.6	0.11	10.9	1.9	12.8	1.9	14.7	1.9
E	14.9	0.11	12.4	2.1	14.6	2.1	16.7	2.1
12	13.2	0.23	10.4	2.1	12.4	2.1	14.2	2.1

Table 6 ***CYLINDER 2. CERN experimental and computed results. Statistical errors only are shown.***

POSITION	EXPERIMENTAL		FLUKA-ISOTROPIC		FLUKA-MIXTURE		FLUKA-LATERAL	
	cts/PIC	err%	cts/PIC	err%	cts/PIC	err%	cts/PIC	err%
CONCRETE TOP								
C	0.813	0.41	0.681	2.3	0.753	2.3	0.881	2.3
D	1.00	0.31	0.788	3.3	0.872	3.3	1.03	3.3
E	1.04	0.24	0.871	3.0	0.977	3.0	1.12	3.0
F	1.21	0.34	0.887	3.6	0.998	3.6	1.15	3.6
H	1.18	0.36	0.912	2.9	1.03	2.9	1.19	2.9
3E	0.801	0.47	0.612	3.0	0.688	3.0	0.794	3.0
CONCRETE SIDE								
R	0.655	0.24	0.580	2.0	0.642	2.0	0.769	2.0
S	1.22	0.14	1.01	1.7	1.12	1.7	1.33	1.7
IRON TOP								
C	20.2	0.03	16.6	1.9	19.7	1.9	22.8	1.9
E	22.0	0.11	18.6	2.1	22.1	2.1	25.5	2.1
12	18.4	0.15	16.2	2.1	19.3	2.1	22.3	2.1

Table 7 ***CYLINDER 1B. CERN experimental and computed results. Statistical errors only are shown.***

POSITION	EXPERIMENTAL		FLUKA-ISOTROPIC		FLUKA-MIXTURE		FLUKA-LATERAL	
	cts/PIC	err%	cts/PIC	err%	cts/PIC	err%	cts/PIC	err%
CONCRETE TOP								
C	0.798	0.34	0.645	2.4	0.601	2.4	0.528	2.4
E	1.01	0.18	0.811	2.9	0.747	2.9	0.663	2.9
CONCRETE SIDE								
R	0.686	0.23	0.615	1.9	0.579	1.9	0.518	1.9
S	1.26	0.37	1.03	1.8	0.970	1.8	0.858	1.8
IRON TOP								
C	20.7	0.06	17.2	2.0	15.6	2.0	14.0	2.0
E	22.3	0.10	19.1	2.1	17.3	2.1	15.6	2.1

Table 8 ***CYLINDER 1. CERN experimental and computed results. Statistical errors only are shown.***

POSITION	EXPERIMENTAL		FLUKA-ISOTROPIC		FLUKA-MIXTURE		FLUKA-LATERAL	
	cts/PIC	err%	cts/PIC	err%	cts/PIC	err%	cts/PIC	err%
CONCRETE TOP								
C	0.685	0.49	0.558	2.6	0.623	2.6	0.752	2.6
D	0.862	0.34	0.634	3.9	0.708	3.9	0.862	3.9
E	0.858	0.35	0.688	2.8	0.780	2.8	0.924	2.8
F	1.02	0.37	0.713	3.6	0.809	3.6	0.969	3.6
H	0.980	0.41	0.717	3.2	0.815	3.2	0.973	3.2
3E	0.679	0.60	0.472	3.0	0.536	3.0	0.641	3.0
CONCRETE SIDE								
R	0.781	0.21	0.597	1.9	0.656	1.9	0.811	1.9
S	1.14	0.23	0.970	1.8	1.09	1.8	1.32	1.8
IRON TOP								
C	14.0	0.07	12.9	1.9	15.1	1.9	17.4	1.9
E	17.4	0.07	14.2	2.1	16.5	2.1	19.1	2.1
12	15.3	0.20	11.6	2.1	13.3	2.1	15.2	2.1